Universal Journal of Carbon Research
https://ojs.wiserpub.com/index.php/ujcr/

Research Article

Improving the mechanical performance of low graphene content epoxy nanocomposites: investigation of hybrid and chemically modified nanofillers

Daniel Belton[1*], Marcin Orawiec[1], Richard Telford[2], Alex Surtees[3]

[1]School of Applied Sciences, University of Huddersfield, Huddersfield, UK
[2]School of Chemistry and Biosciences, Faculty of Life Sciences, University of Bradford, Bradford, UK
[3]School of Archaeological and Forensic Sciences, Faculty of Life Sciences, University of Bradford, Bradford, UK
E-mail: d.j.belton@hud.ac.uk

Received: 15 September 2023; **Revised:** 23 December 2023; **Accepted:** 26 December 2023

Abstract: Graphene is a promising nanofiller for producing polymer nanocomposites with enhanced mechanical, electrical, thermal, electromechanical, and flame retardancy properties, leading to applications in aerospace, automotive, ballistics, medicine, electronics, and smart materials. Solvent-assisted top-down methods, including mechanical exfoliation of graphite, show great potential for scale-up and mass production of graphene dispersions for use in the fabrication of nanocomposites. However, these approaches can suffer from poor efficiency, which limits the concentrations of graphene/polymer dispersions that can be produced using *in situ* methods. As such, it is important to find new ways of making more effective use of these low concentrations of graphene nanofillers. Possible approaches include chemical modification of the graphene or finding synergies with other nanofillers to form hybrid nanocomposites. In this work, we demonstrate results that make use of each approach. Specifically, we demonstrate a low-cost and simple method for producing carbon nanotube dispersions and creating hybrid nanocomposites with substantial enhancements to mechanical properties. We also extend the scope of our previously reported semi-*in situ* exfoliation method by demonstrating its application in the production of a nanocomposite that incorporates chemically modified graphene. The superior mechanical properties exhibited by the nanocomposite are attributed to increased interaction strength between the polymer and nanofiller.

***Keywords*:** graphene, epoxy, nanocomposites, hybrid nanofillers, chemically modified nanofillers

1. Introduction

Graphene combines a range of exceptional electrical, thermal, and mechanical properties within a single material [1-3]. It has demonstrated excellent performance as a nanofiller when combined with a wide range of polymers to form nanocomposites [4-13]. The inclusion of graphene has been shown to confer enhanced properties, including increased mechanical strength and hardness, electrical and thermal conductivity, flame retardancy, high gas barrier performance, and enhanced electromechanical properties [9,14-18]. Graphene-polymer nanocomposites with these enhanced properties have strong prospects for applications in additive manufacturing, aerospace, automotive, ballistics, corrosion protection, medicine, electronics, energy, and smart materials [9,19-26].

DOI: https://doi.org/10.37256/1220233676

A major challenge in the manufacture of graphene-polymer nanocomposites is scaling up the production of the graphene nanofiller at low cost [27,28]. Whilst a range of approaches exist, solvent-assisted exfoliation of graphite offers several advantages and can be incorporated into various approaches such as high shear mixing (HSM), ultrasonication, and three-roll milling/calendering [9,15,29]. Such approaches can yield a combination of graphite microplatelets (GMPs), graphite nanoplatelets (GNPs), few-layer graphene (FLG), and graphene, with unexfoliated material removed [15]. Top-down approaches (graphite to graphene) are simple, low cost, and easier to scale up compared to the alternatives, such as bottom-up approaches (hydrocarbons to graphene) [28,30]. Mechanical solvent-assisted exfoliation does not require the harsh chemical conditions required by chemical exfoliation and it makes use of solvents that can be recovered and recycled rather than reagents that are depleted [15,31]. Furthermore, solvent system viscosity and surface energy can be modified to optimise exfoliation performance [15,29]. To this end, scalable and versatile *in situ* and semi-*in situ* methods have recently been developed, such that the graphite is mechanically exfoliated within a solvent/polymer system [15,29]. The inclusion of the polymer matrix prior to exfoliation allows tuning of the solvent system properties, namely surface energy and viscosity, resulting in stable and homogenous dispersions [15]. However, the approach can suffer from low yields and poor efficiency, severely limiting the concentration of graphene that can be obtained; a common weakness of mechanical exfoliation methods [32,33]. Typically, a solvent-assisted exfoliation method would remedy this by processing large amounts of graphite dispersion, allowing the accumulation of graphene prior to its use as a filler [34]. This is prohibitive for *in situ* or semi-*in situ* methods since the uncured polymer matrix is already present. As such, alternative approaches are required to make more effective use of the limited concentrations of graphene nanofillers attainable.

Carbon nanotubes (CNTs) are known to improve the mechanical properties of polymer nanocomposites [35], with CNT-matrix interactions affecting reinforcement efficacy and, accordingly, these have been subject to extensive prior study [36,37]. Furthermore, graphene has been shown to exhibit synergy with CNTs when both nanofillers are used to fabricate hybrid graphene/CNT polymer nanocomposites [5]. This is due to the formation of a supporting network between the two fillers. Thanks to their high surface area, graphene platelets prevent the agglomeration of CNTs and act as bridging agents [38,39]. Agglomeration of nanofillers significantly deteriorates the performance of nanocomposites leading to inferior mechanical properties and increased percolation thresholds [39]. Recent findings indicate that the enhancement of hybrid nanocomposite properties is most pronounced when the concentration of graphene filler is lower than that of CNTs [39,40]. As such, the low-concentration graphene dispersions obtained via the semi-*in situ* methods, as discussed above, could be ideally suited to the fabrication of hybrid graphene/CNT nanocomposites.

The enhancement of the properties of nanocomposites is strongly dependent on the interaction strength between the filler and polymer matrix [41]. Therefore, one of the most effective methods of increasing the efficacy of graphene filler is to modify its surface with chemical groups that strongly interact with surrounding polymer molecules [41,42]. For example, the variety of oxygen-rich functional groups in graphene oxide (GO) enhance its interaction strength with epoxy matrices [43,44]. However, the sp^2 structure of graphene becomes highly distorted during the oxidation process resulting in decreased mechanical, electrical, and thermal performance of the filler. Furthermore, the increased hydrophilicity of the filler can impede the formation of homogenous dispersions in resins. Wei *et al.* prepared epoxy/GO nanocomposites with varying content of oxygen groups (from 29.4 to 37.5 at%) and examined enhancements to properties [44]; mechanical performance improved with increasing oxygen content to a limit before falling away. This suggests a balance exists between increased load transfer via enhanced nanofiller/matrix interaction and degradation of filler mechanical strength. Overall, it would appear that careful utilisation of mildly oxidized graphene oxide (m-GO) fillers is one potential route to further improving graphene-polymer nanocomposite performance, even with the low concentrations achieved via solvent-assisted mechanical exfoliation. Furthermore, the exfoliation of mildly oxidized graphite as a source for m-GO filler is likely to be more efficient due to increased interlayer spacing [34].

This work demonstrates two approaches to compensate for the low yields of graphene obtained by solvent-assisted graphite exfoliation via high-shear mixing. Firstly, we show how the low-concentration graphene/epoxy dispersions obtained in the semi-*in situ* process can be applied to increase the performance of CNT/epoxy nanocomposites. Secondly, we demonstrate enhancements to the mechanical properties of epoxy/m-GO nanocomposites prepared by the exfoliation of edge-oxidized graphite via high-shear mixing. Epoxy was selected as the host matrix since it has been demonstrated to be a versatile polymer for the creation of nanocomposites [6,8,45,46].

2. Materials and methods

2.1 *Materials*

Graphite flakes (−325 mesh) were obtained from Alfa Aesar. CNTs (single-walled) were obtained from TUBALL™ with a 2 nm diameter, length of at least 5 μm, and iron catalyst content ≤20 wt%. The epoxy resin used in this research was supplied by EasyComposities (EP-L2-S-05) along with a room-temperature curing agent (hardener). Both the epoxy resin and hardener are formulated products. The epoxy resin is based on bisphenol A diglycidyl ether and trimethylolpropane triglycidyl ether. The hardener is marked as 'slow', in reference to the curing speed, and is based on aliphatic and cycloaliphatic amines. Chemicals for the purification and dispersion of CNTs and production of m-GO were obtained from Fisher Scientific: >95% H_2SO_4 (10667422), 70% HNO_3 (N/2300/PB08), 30% H_2O_2 (10121810), 37% HCl (10000180), $KMnO_4$ (207745000), $NaNO_3$ (15603430), isopropanol (IPA) (10588630), tetrahydrofuran (THF) (T/0700/17).

2.2. *Preparation of CNT and hybrid epoxy nanocomposites*

Graphene/epoxy dispersions were obtained using the same semi-*in situ* method presented in our previous work [15], the specific conditions were the same as those used to produce the EpAct120 samples, except that the HSM exfoliation step was run at 15°C for this work instead of the 25°C used previously. Prior to use, CNTs were treated with nitric acid to remove the iron catalyst, in line with a previously proposed protocol [47]. In brief, 1 g of CNTs were refluxed in 150 cm^3 of 3 M $HNO_{3(aq)}$ for 10 hours and then vacuum filtered on a 47 mm circular Durapore® PVDF membrane with 0.22 μm pore size. The residue was washed with deionised water on the membrane with the vacuum on. Washing continued until the filtrate became neutral in pH. The residue underwent a final wash with IPA and was then allowed to air dry. The purified CNTs were dispersed in THF using mechanical stirring at 900 rpm for 20 minutes, followed by 10 minutes of ultrasonication in 20 ml batches using a BioLogics 3000MP ultrasonic probe (300 W) at 55% power amplitude. The CNT/THF dispersion was then combined with either neat epoxy resin (to form samples CNT0.05 and CNT0.1) or graphene/epoxy dispersions (to form sample HC0.05) and mixed with the mechanical stirrer at 600 rpm for 72 hours. The mixtures were placed in a vacuum oven at 60°C for 24 hours to remove the THF. Afterward, the epoxy/nanofiller dispersions were placed in a 45 Hz ultrasonic bath at 50°C for 5 hours and then mixed with the mechanical stirrer at 600 rpm until cast (at least another 24 hours). The steps of the production process are summarised visually in Figure 1. The final epoxy/nanofiller dispersions were black in appearance with a metallic reflection and did not contain any visible CNT clusters, confirmed by spreading a small portion on a glass slide. Epoxy/nanofiller dispersions were manually mixed with the hardener (100:30 mass ratio) and cast into dog-bone shaped silicone moulds, degassed in a vacuum desiccator, and cured at room temperature overnight.

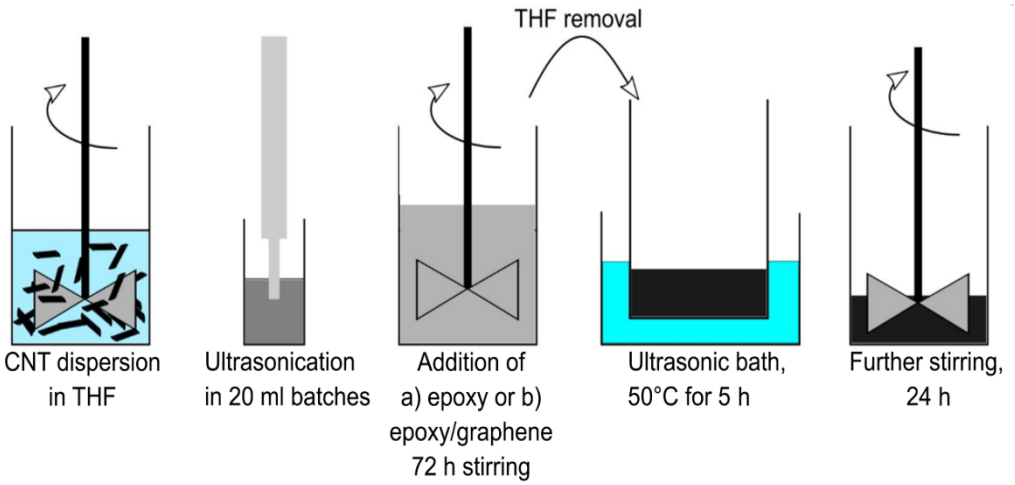

Figure 1. Preparation of epoxy nanocomposites: a) CNT nanofiller; b) hybrid nanocomposites containing CNTs and graphene nanofillers.

2.3. *Preparation of epoxy/m-GO nanocomposite*

Edge-oxidized graphite (EOG) was prepared using a scaled-up version of a previously proposed method [48]. In brief, 10 g of graphite and 1 g of $NaNO_3$ were dispersed/dissolved in a 230 cm^3 solution in H_2SO_4 (>95%) using an overhead Teflon stirrer. An ice bath was used to maintain the temperature at 20°C, while 8 g $KMnO_4$ was gradually added. The mixture was heated to 35°C and held for 30 minutes. 460 cm^3 of deionised was gradually added to the mixture and stirred for 15 minutes. The mixture was then poured into a beaker containing 1400 cm^3

of deionised water and 75 cm^3 of concentrated H_2O_2. The mixture was allowed to sediment, and the liquid was decanted. The wet slurry was centrifuged for 15 minutes at 3000 g and then dispersed in 5 litres of 5% $HCl_{(aq)}$ and left overnight to sediment. The slurry was centrifuged and redispersed in deionised water three times. The slurry was then transferred to dialysis membranes and placed in a 10 litre bucket filled with deionised water and stirred. During the dialysis, water was regularly changed, and its conductivity was monitored. The process was conducted for around 10 days until the conductivity of water was below 2 µS. The contents of the membranes were filtered using filter paper, washed with water and methanol, and dried to produce the final EOG product.

The m-GO/epoxy composites were prepared as follows. EOG was exfoliated in batches of 2 g in 100 cm^3 of IPA in a 150 cm^3 beaker at 15°C using a L5M Silverson High Shear Mixer set at 9500 rpm for 120 minutes. The dispersion was then transferred to 50 cm^3 falcon tubes and centrifuged at 2100 g for 30 minutes. The supernatant was collected and mixed with 12 g of epoxy resin. The IPA was then removed using a rotary evaporator. The steps of the production process are summarised visually in Figure 2. The final epoxy/m-GO dispersion was manually mixed with the hardener (100:30 mass ratio) and cast into dog-bone shaped silicone moulds, degassed in a vacuum desiccator, and cured at room temperature overnight.

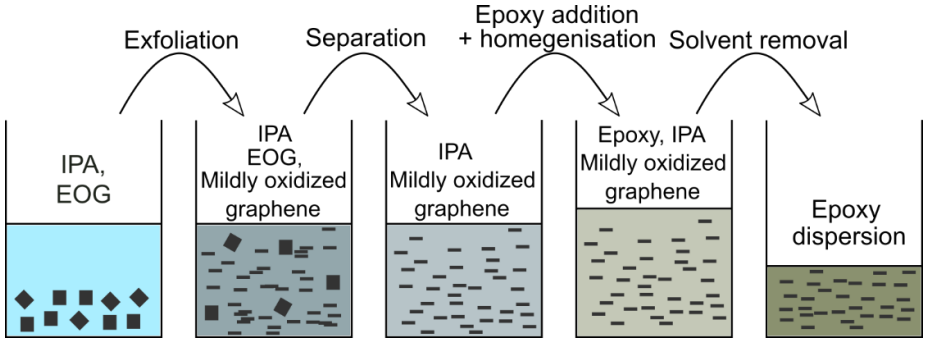

Figure 2. Production of mildly oxidised graphene epoxy composites via liquid exfoliation.

2.4. *Analysis*

The concertation of graphene species in the dispersions was determined using UV-Vis absorption measurements at 660 nm. The absorption coefficients were determined experimentally: 1099 ± 32 g·mg^{-1}·m^{-1} for graphene dispersions used to make hybrid composite [15] and 1234 ± 52 g·mg^{-1}·m^{-1} for m-GO/IPA dispersions. EOG was analysed using a Bruker D2 Phaser X-ray powder diffractometer (XRD) and Cu-K_α radiation (λ = 1.54184 A˚) source. A Renishaw inVia Raman Microscope, with a 520 nm laser, was used to assess the structure of m-GO produced. The size distributions of graphitic platelets in the supernatants were measured using a Malvern Mastersizer 2000. An Instron universal testing machine was used to test the mechanical properties of the nanocomposites. Three tensile properties of the nanocomposites were determined and compared with neat epoxy resin: Young's modulus (E), ultimate tensile strength (UTS), and elongation at break (ε_{max}). Young's modulus determines the stiffness of a material and is calculated as a slope of a linear region of the stress-strain curve. UTS is the maximum stress that a material can withstand before fracture, and ε_{max} is the maximum extension before fracture. The properties of nanocomposites cast as dog-bone shapes were measured using an Instron universal testing machine. The dimensions of the dog-bone shapes were measured before the tensile tests with callipers to calculate the cross-sectional area of the samples. The applied measurement gap was 75 mm, and the elongation speed was set to 0.3 mm min^{-1}. The software recorded force versus displacement curves, and these were transformed into stress versus strain curves to obtain E, UTS, and ε_{max}. All the calculations were conducted using a MATLAB program. All specimens were measured in triplicate with mean values reported along with standard deviation. The hardness measurements of composites were conducted using a Vickers micro indentation tester according to ISO 6507-1 with an applied load of 300 gf for 15 seconds.

3. Results and Discussion

3.1. *CNT and hybrid nanocomposites*

CNT/epoxy nanocomposites containing 0.05 and 0.1 wt% of the filler were prepared according to the method described above, referred to as CNT0.05 and CNT0.1 respectively. Hybrid nanocomposites containing 0.05 wt% of CNT and 8×10^{-3} % graphene were also prepared according to the method described above and are referred to as HC0.05. The tensile and hardness properties of the nanocomposites are reported in Table 1 and the tensile

properties alone are compared in Figure 3. Typical stress-strain curves for each sample series are presented in Figure 4.

Table 1. Measured properties of the CNT and hybrid epoxy nanocomposites.

Sample	Graphene /10^{-2} %	CNT /%	E^a /MPa	UTS^b /MPa	$\varepsilon_{max}{}^c$ /%	HV0.3^d
CNT0.05	n/a	0.05	2312 ± 252	41.0 ± 16.9	1.8 ± 0.5	19.4 ± 0.3
CNT0.1	n/a	0.1	2386 ± 214	49.2 ± 9.1	2.2 ± 0.9	19.8 ± 0.5
HC0.05	0.8 ± 0.2	0.05	2308 ± 45	49.9 ± 3.6	2.4 ± 0.2	19.6 ± 0.3
Neat epoxy	n/a	n/a	2217 ± 119	45.5 ± 3.5	2.2 ± 0.2	18.3 ± 0.2

[a]Young's modulus, [b]ultimate tensile strength, [c]elongation at break, [d]Vickers hardness.

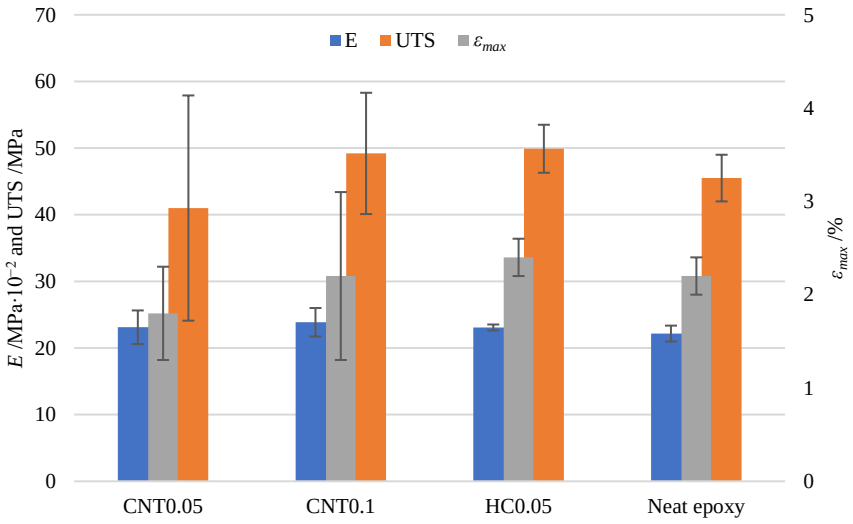

Figure 3. Comparison of the tensile and hardness properties of CNT and hybrid epoxy nanocomposites.

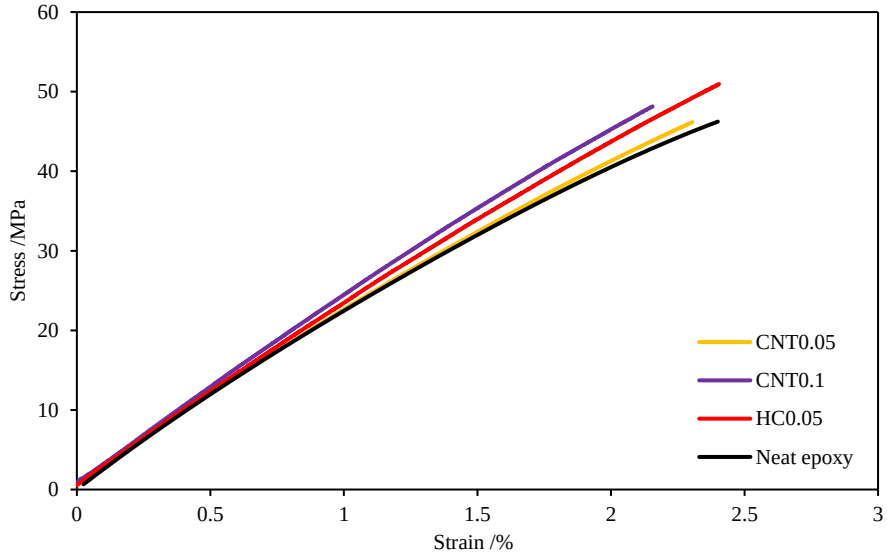

Figure 4. Examples of strain-stress curves of CNT/epoxy and hybrid epoxy nanocomposites.

The inclusion of either nanofiller improves the hardness of the material, as shown by the Vickers hardness data in Table 1. The tensile properties of both CNT nanocomposites (CNT0.05 and CNT0.1) exhibit considerable variability, as indicated by the large uncertainties in Table 1 and Figure 3. This could potentially be due to the agglomeration of the nanofiller or hindered degassing resulting in the presence of air bubbles. The latter is thought to be a dominating factor since the viscosity of the CNT/epoxy dispersion was significantly increased compared to epoxy/graphene dispersions, which forced the time for degassing to be reduced by around 30% to ensure reliable casting. The uncertainties of Young's modulus for both CNT nanocomposites are around ±10%. In terms of UTS,

CNT0.05 shows a higher degree of variability than CNT0.1, with uncertainties in UTS of ±41% and ±18%, respectively. In contrast, for elongation at break, CNT0.05 shows a lower degree of variability than CNT0.1, with uncertainties in elongation at break of ±28% and ±41%, respectively. It is difficult to make exact comparisons with such a spread of data; nonetheless, some general inferences can be drawn. First of all, the rigidity, tensile strength, and elongation at break of CNT composites increase with the increasing filler content, which corresponds with the reports of other researchers [6]. At 0.05% CNTs, the composites exhibit lower tensile strength and elongation at break than neat epoxy; however, they are more rigid. On average, the CNT0.1 composites have an improved Young's modulus and UTS of 8% each, compared to neat epoxy; however, elongation at break is unchanged. Considering the amount of effort and extra solvents needed to disperse CNTs in epoxy resin, it is not a profound improvement. As mentioned above, the high degree of uncertainty in results, and the limited improvements in properties, are potentially attributable to issues with degassing and agglomeration during the curing process, and these factors would merit further investigation.

The spread of Young's modulus and UTS data for the hybrid composites (HC0.05) is lower compared to the CNT composites and is comparable to that reported in our previous work, at around ±10% or less [15]. It is unlikely that the degassing process of the hybridised composites was vastly different from the composites with CNTs alone. The epoxy/graphene dispersions are subjected to rotary evaporation before CNTs are dispersed in them. However, the nanofiller/epoxy dispersions for CNT0.05, CNT0.1, and HC0.05 each spend 24 hours under vacuum at 60°C to remove any traces of THF; as such, the final amount of trapped air in the hybrid dispersions (HC0.05) should not be greatly affected by the prior treatment of graphene dispersions. The presence of GMPs, GNPs, and FLG can potentially prevent the re-agglomeration of CNTs in the epoxy matrix as these materials can interact via π-π stacking resulting in more reproducible results [39,49]. The hybrid nanocomposites (HC0.05) exhibit a comparable rigidity and tensile strength to the CNT0.1 nanocomposite, but demonstrate a 9% improvement in elongation at break, even though the CNT content is 50% lower in HC0.05 compared to CNT0.1. These results demonstrate that graphene dispersions obtained through the semi-*in situ* exfoliation process can aid the dispersion of CNTs to produce hybrid nanocomposites with enhanced properties. Furthermore, this method could reduce the amount of CNTs needed in a composite, which could be highly beneficial for large-scale manufacture, since dispersing CNTs in epoxy is not straightforward. Furthermore, the manufacturing process of graphene/epoxy dispersions with epoxy/acetone systems is relatively simple compared to the dispersing requirements of CNTs. Consequently, the use of graphene/epoxy dispersions should have a lower impact on the cost of production compared to incorporating CNTs.

3.2. *Characterization of EOG*

Edge-oxidized graphite (EOG) was synthesized via mild oxidation of graphite powder using a modified *Hummers'* method, as described above. The XRD pattern for EOG presented in Figure 5 incorporates a broad amorphous peak superimposed over the entire signal range and indicates that the mild oxidation has perturbed the crystalline structure of the graphite. Furthermore, the 002 graphite peak has shifted from 26.5° to 25.8° as a result of the increased graphite interlayer spacing [48]. An average 2θ value from four XRD patterns from two different batches of EOG is 25.8° ± 0.2°, which corresponds to an increase in interlayer spacing from 0.336 nm (for pristine graphite) to 0.345 nm ± 0.005 nm. The peak at 12.9° is due to the partial intercalation of micrographite platelets with water [48]. It is challenging to assess whether some particles are fully intercalated and some just mildly oxidized or if partial intercalation is present in all of the graphite platelets. The interlayer spacing calculated from the 12.9° peak position is 0.686 nm ± 0.014 nm.

The method of synthesis was scaled up from a method proposed by Bai *et al* [48]. Interestingly, the 25.8° peak was also reported in their work, along with a smaller peak between 10° and 15° with much lower intensity than the peak reported here. When they examined the XRD pattern for GO, they reported only one peak at 11.1°, which corresponds to fully intercalated graphite with an interlayer spacing of 0.79 nm. These results suggest that the EOG produced in this work is not fully oxidized but that it is potentially oxidized to a greater extent than the EOG produced by Bai *et al* [48]. There are two critical stages during the scaled-up synthesis which could have resulted in enhanced oxidation. Firstly, the synthesis was conducted in five times the volume of concentrated H_2SO_4, resulting in five times more water in the last stage of synthesis. The heat generated by mixing this larger volume of concentrated acid with water could have accelerated the oxidation of graphite platelets [50]. Secondly, the increased amount of H_2O_2 used for quenching could have facilitated the intercalation and partial exfoliation of oxidized graphite [51].

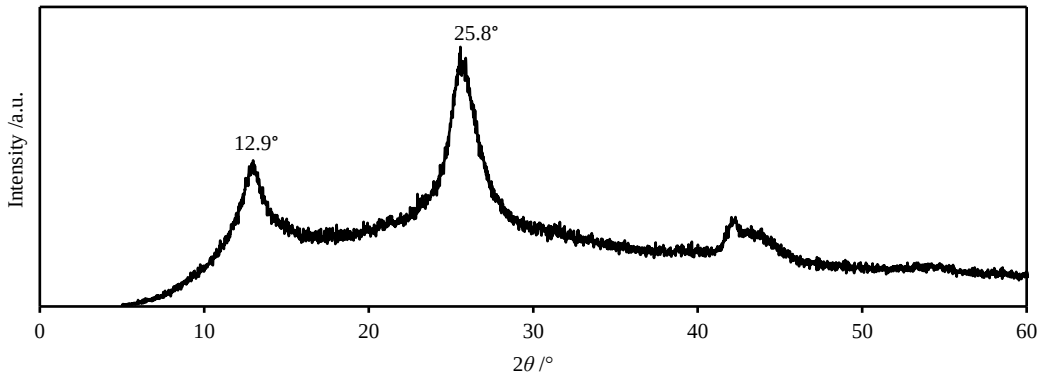

Figure 5. XRD pattern of EOG. Peaks at 12.9° and 25.8° are (002) diffraction lines of respectively fully intercalated graphite and mildly oxidized phase. The peaks visible between 40 and 50° correspond to (100) and (101) diffraction lines of graphite.

3.3. *Epoxy/m-GO nanocomposites*

The exfoliation of EOG was conducted in IPA, without epoxy present, which has several benefits. IPA exhibits preferential surface properties for the exfoliation of EOG, resulting in stable dispersions [48]. Adding epoxy to the IPA is likely to create less favourable wetting properties for exfoliation, meaning the process would be less efficient compared to using the neat polar solvent. Furthermore, IPA has a much better safety profile compared to many other solvents recommended in the literature for the exfoliation of graphite [30,52]. Finally, several routes for the effective recovery and reuse of IPA have been demonstrated [53].

The HSM process was conducted on IPA/EOG dispersions containing 2 wt% EOG for 120 minutes at 15°C. Then the resulting dispersions were centrifuged for 30 minutes to obtain final m-GO dispersions.

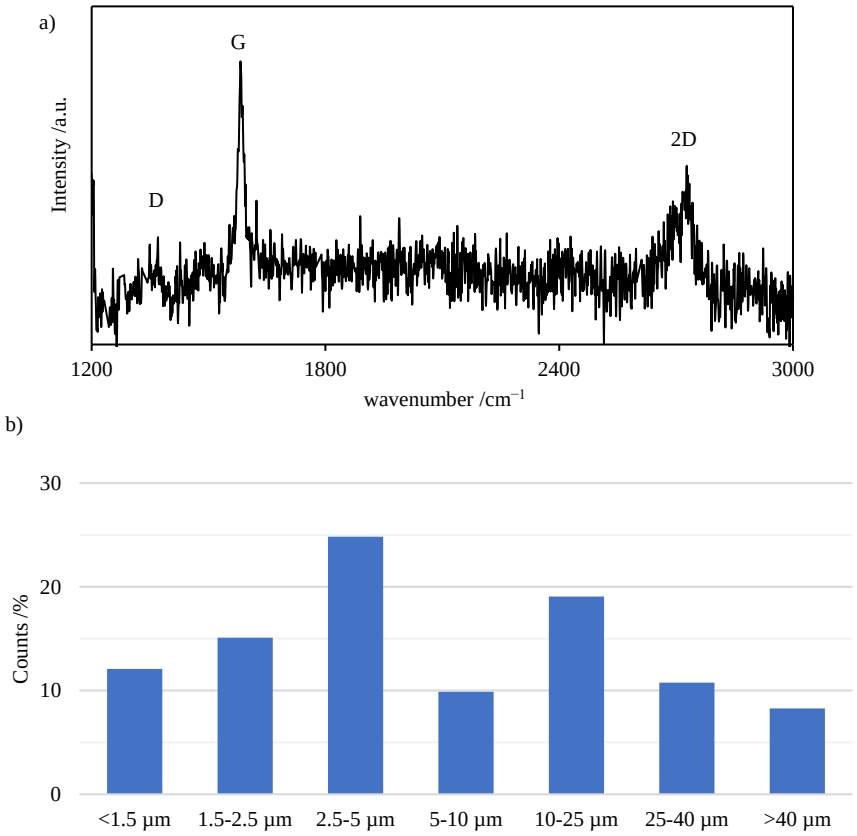

Figure 6. m-GO characterisation (a) Raman spectrum of m-GO on a filter membrane, (b) Average size distribution graph of m-GO dispersion.

The average concentration of m-GO dispersions was 0.015 ± 0.004 mg·g$^{-1,}$ which corresponds to an average yield of 0.08 ± 0.02 %, which is typical for graphite exfoliation [54]. Raman spectra of m-GO proved challenging

to register, perhaps due to the number of defects introduced. Nevertheless, the spectrum presented in Figure 6 a) contains characteristic G and 2D peaks and perhaps a small D peak, suggesting that at least some of the graphitic structure is persevered [55]. Retaining this graphene/graphitic structure could be advantageous since graphene has a much higher intrinsic strength compared to graphene oxide [56]. It is not possible to draw any further conclusions from the Raman spectrum, since the intensity of the peaks is barely above the baseline. The size of m-GO platelets is significantly larger compared to platelets obtained in our previous work [15]. The average Sauter mean diameter calculated by MasterSizer is 3.6 microns, which is over three times greater than observed in our previous work [15]. This appears to be an additional benefit of the current approach since increasing the lateral size of graphene-based nanofillers can further improve nanocomposite properties [34]. The size distribution presented in Figure 6 b) suggests a bimodal distribution with over 50% of platelets smaller than 5 microns and nearly 40% of platelets larger than 10 microns.

Nanocomposites containing 1.1×10^{-2} wt% of m-GO were prepared according to the method described above and are referred to as EpmGO. The tensile and hardness properties of the EpmGO nanocomposites are reported in Table 2, along with comparator values for neat epoxy and EpAct120. EpAct120 is a nanocomposite prepared under very similar conditions to EpmGO and with a similar level of filler content, as reported in our previous work [15], the key difference is that EpAct120 contains a graphene-based nanofiller that has not been oxidised. Furthermore, the EpAct120 platelet size is much smaller, at 0.22 microns [15]. Typical stress-strain curves for each sample series are presented in Figure 7.

Table 2. Measured properties of EpmGO nanocomposites, including comparison with EpAct120 and neat epoxy.

Sample	Filler /10^{-2} %	E^a /MPa	UTS[b] /MPa	$\varepsilon_{max}{}^c$ /%	HV0.3[d]
EpmGO	1.1 ± 0.3	2395 ± 29	62.2 ± 2.8	3.0 ± 0.2	20.0 ± 0.4
EpAct120[e]	1.3 ± 0.5	2380 ± 50	50.3 ± 4.1	2.4 ± 0.4	19.0 ± 0.3
Neat epoxy	n/a	2217 ± 119	45.5 ± 3.5	2.2 ± 0.2	18.3 ± 0.2

[a]Young's modulus, [b]ultimate tensile strength, [c]elongation at break, [d]Vickers hardness, [e]results from previous work [15].

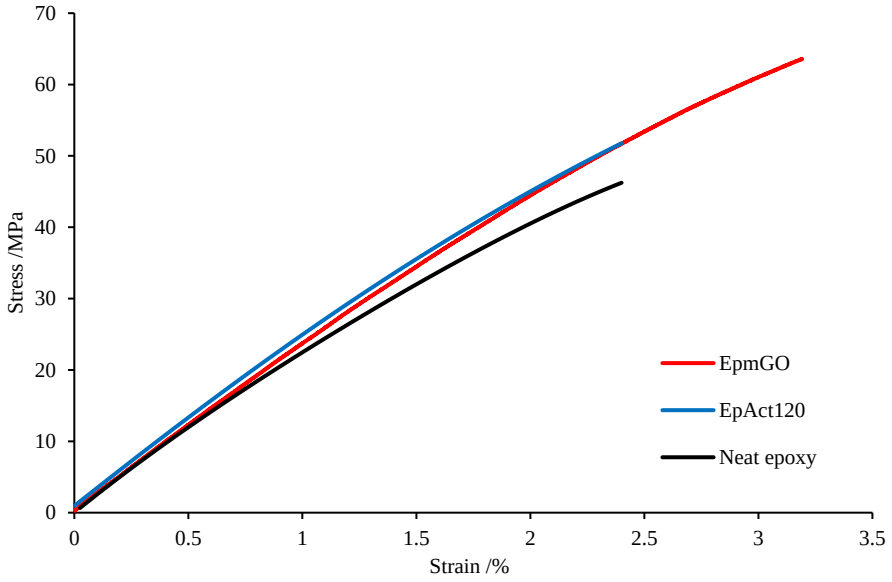

Figure 7. Typical stress-strain curves of EpmGO nanocomposite, neat epoxy, and EpAct120.

The EpmGO nanocomposites exhibit the most prominent enhancement of all tested properties amongst all studied nanocomposites in this work. The increase in Young's modulus, UTS, elongation at break, and Vickers hardness are respectively 8%, 37%, 36%, and 9%, versus neat epoxy. Moreover, the uncertainty of the calculated tensile properties is the lowest among all the tested samples, which affirms the repeatability of this method. Given that the mean platelet size of the EpmGO is approximately sixteen times larger than that of the platelets in EpAct120, the composite would be expected to have a much higher Young's modulus and reduced flexibility [34], however, this behaviour is not observed here. Instead, the mechanical property profile is more in line with previous work that used chemically modified nanofillers, with the potential for stronger interaction or even cross-linking with the polymer matrix [57,58]. In one case, graphene platelets modified with polybenzimidazole exhibited a

12%, 20%, and 4.4% increase in Young's modulus, UTS, and elongation at break respectively, versus neat epoxy, but required ten times the level of nanofiller used in EpmGO to achieve this [57]. In another example, epoxy chains were grafted onto GO, resulting in a 6.3%, 79%, and 72% increase in Young's modulus, UTS, and elongation at break respectively [58]. Again, this required ten times the level of nanofiller used in EpmGO. Further examples utilise graphene grafted with various oxygen and amine functional groups, resulting in nanocomposites with a similar improvement in mechanical properties [43,59]. Overall, the results indicate that the improved performance of EpmGO is due to the introduction of functional groups during the mild oxidation process and that these groups participate in the curing process either by forming covalent bonds with the epoxy or by increasing the strength of interaction between graphene and epoxy resins with H-bonds or other polar interactions.

3.4. *Comparison with literature*

Table 3 correlates the improvement in tensile properties of epoxy resins achieved in this research with results reported in previous investigations of epoxy nanocomposites with low filler content.

Table 3. Comparison of the enhancements of mechanical properties of the epoxy nanocomposites with the literature.

Filler/sample	Filler wt. content (%)	*E* increase (%)	UTS increase (%)	ε_{max} increase (%)	Ref.
CNT0.05	0.05	4.3	−9.9	−18.2	This work
CNT0.1	0.1	7.6	8.1	0.0	
HC0.05 (CNT/Graphene)	0.05/0.01	4.1	9.7	9.1	
EpmGO	0.01	8.0	36.7	36.4	
FLG/GMPs/GNPs EpNMPWc60	0.02	3.0	−4.2	4.5	Our previous work[15]
FLG/GMPs/GNPs EpNMPT15	0.01	9.4	3.1	4.2	
FLG/GNPs	0.1	2	2	11	[60]
FLG/GNPs	1	24	−41	-	[61]
GMPs	2.5	25	9	5	[62]
Expanded GIC (GNPs and FLG)	0.5	3	−5	-	[63]
GO	0.1	31	40	-	[64]
GO	0.1	12	4	-	[65]
GO	0.1	3.8	35	13	[58]
GO	0.1	7	8	22	[43]
Covalently functionalized GO	0.1	6.3	79	72	[58]
Covalently functionalized expanded GIC	0.1	12	20	4.4	[57]
SWCNTs	0.1	−12	4	−16	[66]
SWCNTs	0.1	3	11	-	[64]
MWCNTs	0.3	-	17	−14	[40]
FMWCNTs/FLG	0.05/0.05	9	~ 25	~ −20	[67]
MWCNTs/GNPs	0.24/0.26	~ 11	14	~ −25	[68]
MWCNTs/FLG	0.3 (1/1)	-	3	−13	[40]
MWCNTs/FLG	0.3 (3/1)	-	29	−14	[40]

Abbreviations: CNTs, carbon nanotubes; FLG, few-layer graphene; FMWCNTs, functionalized MWCNTs; GMPs, graphite microplatelets; GNPs, graphite nanoplatelets; GIC, graphite intercalation compound; GO, graphene oxide; MWCNTs, multi-walled CNTs; SWCNTs, single-walled CNTs; UTS, ultimate tensile strength.

The mechanical properties of nanocomposites with CNTs reported in this work have high uncertainties and the changes in properties shown in Table 8 for CNT0.05 and CNT0.1 should be treated with caution. They exhibit similar changes and issues to those exhibited by nanocomposites reported elsewhere that incorporate CNTs. For example, Li *et al.* reported an 8% increase in Young's modulus, a 15% improvement in UTS, and a 16% reduction in elongation at break for epoxy composites containing 0.5 wt% multi-walled carbon nanotubes (MWCNTs). A similar reduction in elongation at break was also reported by Dutta *et al.* for epoxy composites containing single-walled carbon nanotubes (SWCNTs) at 0.1 wt%. This issue was further exacerbated by increasing the nanotube content, with epoxy containing 1 wt% SWCNTs showing a 59% reduction in elongation at break. Both Li *et al.* and Dutta *et al.* attribute the observed reductions in elongation at break to agglomeration of nanofillers, resulting in voids and defects that cause localised stress concentration and ultimately increased brittleness of the composites. Previously reported hybrid nanocomposites suffered similar issues with compromised elongation at break and brittleness. Data presented by Moosa *et al.* suggests that hybrid composites containing a combination of functionalised MWCNTs and GNPs have a reduced elongation of break of anywhere between 12 to 18%. Li et al. observed that materials containing 0.24 wt% MWCNTs and 0.26 wt% GNPs had a 28% reduction in elongation

at break. These observations are again attributed to increased brittleness resulting from flaws that localise stress concentration. In sharp contrast, the hybrid nanocomposites produced in this work (HC0.05) exhibit increased ultimate tensile strength without compromising elongation of break. As such, the approach taken here provides a promising route to producing hybrid nanocomposites with improved strength without the brittleness that has compromised previously reported materials.

Nanocomposites prepared with m-GO (EpmGO) successfully compete in terms of tensile properties with nanocomposites reported elsewhere that incorporate modified graphene. Nanocomposites containing 0.1 wt% GO prepared by Wan *et al.* and Li *et al.* exhibit a lower overall increase in all tensile properties compared to EpmGO samples [43,58]. Wan *et al.* also functionalized GO platelets with epoxy chains to improve interaction with the epoxy resin, resulting in nanocomposites that surpassed the performance of EpmGO, with a 79% improvement in tensile strength and 72% improvement in elongation at break, but this required ten times the filler loading of that used for EpmGO [58]. Zhang *et al.* prepared nanocomposites containing 0.1 wt% graphene platelets modified with polybenzimidazole but observed only limited improvements in mechanical performance, with an increase in tensile strength of 20% and elongation at break of 4.4%, which are outperformed by EpmGO, even though its filler content is a factor of ten lower [57].

4. Conclusions

Two approaches to improving the mechanical performance of low filler content graphene/epoxy nanocomposites were investigated: mild oxidation of the graphene filler and creating hybrid nanocomposites that incorporate CNTs along with graphene. The nanocomposites exhibited improved mechanical properties and hardness, therefore demonstrating the utility of these approaches for improving the mechanical performance of low filler content graphene/epoxy nanocomposites. As such, these approaches could serve as viable routes for the scalable industrial production of epoxy/graphene nanocomposites, especially, given their versatility and simplicity.

Focusing on the production of the hybrid CNT/graphene epoxy nanocomposites, the application of the epoxy/acetone systems in the semi-*in situ* exfoliation process demonstrates several potential advantages. Firstly, acetone is inexpensive, and straightforward to recycle, making this method economically viable. Secondly, the application of graphene/epoxy dispersions to the production of CNT nanocomposite counteracted the deterioration of tensile properties observed with nanocomposites that incorporated CNTs alone. As a result, a material with better properties than a CNT nanocomposite containing twice as much filler was obtained. As such, the proposed method could aid the manufacturing process of CNT/epoxy nanocomposites by decreasing the concentration of CNTs while preserving the mechanical properties of the nanocomposite.

The nanocomposites prepared from functionalized graphene dispersions (EpmGO) exhibit a notable improvement of tensile properties at low filler content without becoming brittle; 37% increased tensile strength and 36% increased elongation at break at 0.01 wt% of the filler and only an 8% increased Young's modulus. This enhancement is comparable with some reported in the literature for nanocomposites containing ten times more filler. Results show that the EOG used to produce the nanocomposites contains oxygen-based functional groups on the surface and is at least partially exfoliated, as shown by XRD studies. The introduced functional groups give EOG two crucial advantages over natural graphite. Firstly, EOG is hydrophilic, meaning that exfoliation is possible in solvents that have a better safety and environmental profile compared to solvents more commonly used for graphene exfoliation. Secondly, the new functional groups can interact with the epoxy matrix either by forming covalent bonds or by H-bonds and dipole-dipole interactions, which improves load transfer and nanofiller efficacy.

Acknowledgments

The authors gratefully acknowledge financial support from the School of Applied Sciences, University of Huddersfield.

Conflict of interest

There is no conflict of interest for this study.

References

[1] Kumar, A.; Sharma, K.; Dixit, A.R. A review on the mechanical and thermal properties of graphene and graphene-based polymer nanocomposites: understanding of modelling and MD simulation. *Mol. Simul.* **2019**, *46*, 136–154, https://doi.org/10.1080/08927022.2019.1680844.

[2] Goodrum, R.; Weldekidan, H.; Li, H.; Mohanty, A.K.; Misra, M. Graphene-based nanostructures from green processes and their applications in biomedical sensors. *Adv. Ind. Eng. Polym. Res.* **2023**, https://doi.org/10.1016/j.aiepr.2023.03.001.

[3] Ishraq, S.; Liu, Y. Synthesis, Characterization and Bioapplications of Pristine Graphene: A Review. *Univers. J. Carbon Res.* **2023**, 1–21, https://doi.org/10.37256/ujcr.1120231898.

[4] Hu, K.; Kulkarni, D.D.; Choi, I.; Tsukruk, V.V. Graphene-polymer nanocomposites for structural and functional applications. *Prog. Polym. Sci.* **2014**, *39*, 1934–1972, https://doi.org/10.1016/j.progpolymsci.2014.03.001.

[5] Kumar, A.; Sharma, K.; Dixit, A.R. Carbon nanotube- and graphene-reinforced multiphase polymeric composites: review on their properties and applications. *J. Mater. Sci.* **2019**, *55*, 2682–2724, https://doi.org/10.1007/s10853-019-04196-y.

[6] Singh, N.P.; Gupta, V.; Singh, A.P. Graphene and carbon nanotube reinforced epoxy nanocomposites: A review. *Polymer* **2019**, *180*, 121724, doi:10.1016/j.polymer.2019.121724.

[7] Gürler, N.; Torğut, G. Graphene-reinforced potato starch composite films: Improvement of mechanical, barrier and electrical properties. *Polym. Compos.* **2020**, *42*, 173–180, https://doi.org/10.1002/pc.25816.

[8] G., A.K.; K., K. Mechanical, ballistic impact, and water absorption behavior of luffa/graphene reinforced epoxy composites. *Polym. Compos.* **2020**, *41*, 4716–4726, https://doi.org/10.1002/pc.25745.

[9] Pérez, I.; Flores, S.; Ortiz, C.; Rivero, M.; Corona, J.E.; Oliva, A.I.; Avilés, F. Processing-structure-property relationship of multilayer graphene sheet thermosetting nanocomposites manufactured by calendering. *Polym. Compos.* **2022**, *43*, 2150–2162, https://doi.org/10.1002/pc.26528.

[10] Shirvanimoghaddam, K.; Balaji, K.; Ahmadi, M.; Nazarloo, H.A.; Yadav, R.; Zabihi, O.; Egan, B.; Adetunji, P.; Naebe, M. Strategies to resolve intrinsic conflicts between strength and toughness in polyethylene composites. *Adv. Ind. Eng. Polym. Res.* **2023**, https://doi.org/10.1016/j.aiepr.2023.03.004.

[11] Ullah, M.W.; Alabbosh, K.F.; Fatima, A.; Islam, S.U.; Manan, S.; Ul-Islam, M.; Yang, G. Advanced biotechnological applications of bacterial nanocellulose-based biopolymer nanohybrids: A review. *Adv. Ind. Eng. Polym. Res.* **2023**, https://doi.org/10.1016/j.aiepr.2023.07.004.

[12] Karchoubi, F.; Ghotli, R.A.; Pahlevani, H.; Salehi, M.B. New insights into nanocomposite hydrogels; a review on recent advances in characteristics and applications. *Adv. Ind. Eng. Polym. Res.* **2023**, https://doi.org/10.1016/j.aiepr.2023.06.002.

[13] Ollengo, M.A. Graphene Oxide/Nanocrystalline Cellulose Composite: A Facile Phase Modulator. *Univers. J. Carbon Res.* **2023**, 63–76, https://doi.org/10.37256/ujcr.1120232216.

[14] Liu, Q.; Zhao, Y.; Gao, S.; Yang, X.; Fan, R.; Zhi, M.; Fu, M. Recent advances in the flame retardancy role of graphene and its derivatives in epoxy resin materials. *Compos. Part A: Appl. Sci. Manuf.* **2021**, *149*, 106539, https://doi.org/10.1016/j.compositesa.2021.106539.

[15] Orawiec, M.; Belton, D.; Telford, R.; Surtees, A. Application of semi-*in situ* liquid exfoliation of graphite to the scalable production of graphene-epoxy nanocomposites. *Polym. Compos.* **2020**, *41*, 4933–4944, https://doi.org/10.1002/pc.25764.

[16] Sun, X.; Huang, C.; Wang, L.; Liang, L.; Cheng, Y.; Fei, W.; Li, Y. Recent Progress in Graphene/Polymer Nanocomposites. *Adv. Mater.* **2020**, *33*, e2001105, https://doi.org/10.1002/adma.202001105.

[17] Wang, M.; Yin, G.-Z.; Yang, Y.; Fu, W.; Palencia, J.L.D.; Zhao, J.; Wang, N.; Jiang, Y.; Wang, D.-Y. Bio-based flame retardants to polymers: A review. *Adv. Ind. Eng. Polym. Res.* **2023**, *6*, 132–155, https://doi.org/10.1016/j.aiepr.2022.07.003.

[18] Mandlekar, N.; Joshi, M.; Butola, B.S. A review on specialty elastomers based potential inflatable structures and applications. *Adv. Ind. Eng. Polym. Res.* **2021**, *5*, 33–45, https://doi.org/10.1016/j.aiepr.2021.05.004.

[19] Kausar, A.; Rafique, I.; Muhammad, B. Aerospace Application of Polymer Nanocomposite with Carbon Nanotube, Graphite, Graphene Oxide, and Nanoclay. *Polym. Technol. Eng.* **2017**, *56*, 1438–1456, https://doi.org/10.1080/03602559.2016.1276594.

[20] Govindaraj, P.; Fox, B.L.; Aitchison, P.; Hameed, N. A Review on Graphene Polymer Nanocomposites in Harsh Operating Conditions. *Ind. Eng. Chem. Res.* **2019**, *58*, 17106–17129, https://doi.org/10.1021/acs.iecr.9b01183.

[21] P.P. Das, V. Chaudhary, Application of graphene-based biopolymer nanocomposites for automotive and electronic based components, in: Graphene Based Biopolymer Nanocomposites, Springer, Singapore; 2021. p.311-323.

[22] Zhang, X.; Samorì, P. Graphene/Polymer Nanocomposites for Supercapacitors. *Chemnanomat* **2017**, *3*, 362–372, https://doi.org/10.1002/cnma.201700055.
[23] Silva, M.; Pinho, I.S.; Covas, J.A.; Alves, N.M.; Paiva, M.C. 3D printing of graphene-based polymeric nanocomposites for biomedical applications. *Funct. Compos. Mater.* **2021**, *2*, 1–21, https://doi.org/10.1186/s42252-021-00020-6.
[24] Madaswamy, S.L.; Keertheeswari, N.V.; Alothman, A.A.; Al-Anazy, M.M.; Alqahtani, K.N.; Wabaidur, S.M.; Dhanusuraman, R. Fabrication of nanocomposite networks using Pd nanoparticles/Polydiphenylamine anchored on the surface of reduced graphene oxide: An efficient anode electrocatalyst for oxidation of methanol. *Adv. Ind. Eng. Polym. Res.* **2021**, *5*, 18–25, https://doi.org/10.1016/j.aiepr.2021.08.001.
[25] Verma, C.; Quraishi, M.; Alfantazi, A.; Rhee, K.Y. Biodegradable synthetic polymers in sustainable corrosion protection: Present and future scenarios. *Adv. Ind. Eng. Polym. Res.* **2023**, *6*, 407–435, https://doi.org/10.1016/j.aiepr.2023.04.005.
[26] Sivadas, B.; Ashcroft, I.; Khlobystov, A.; Goodridge, R. Laser sintering of polymer nanocomposites. *Adv. Ind. Eng. Polym. Res.* **2021**, *4*, 277–300, https://doi.org/10.1016/j.aiepr.2021.07.003.
[27] Zhu, Y.; Ji, H.; Cheng, H.-M.; Ruoff, R.S. Mass production and industrial applications of graphene materials. *Natl. Sci. Rev.* **2018**, *5*, 90–101, doi:10.1093/nsr/nwx055.
[28] I. Srivastava, M.A. Rafiee, F. Yavari, J. Rafiee, N. Koratkar, Epoxy nanocomposites: Graphene a promising filler, in: Graphite, Graphene, and Their Polymer Nanocomposites, CRC Press, Boca Raton; 2012. p.315-351.
[29] Li, Y.; Zhang, H.; Bilotti, E.; Peijs, T. Optimization of Three-Roll Mill Parameters for In-Situ Exfoliation of Graphene. *MRS Adv.* **2016**, *1*, 1389–1394, https://doi.org/10.1557/adv.2016.191.
[30] Yi, M.; Shen, Z. A review on mechanical exfoliation for the scalable production of graphene. *J. Mater. Chem. A* **2015**, *3*, 11700–11715, https://doi.org/10.1039/c5ta00252d.
[31] Danial, W.H.; Norhisham, N.A.; Noorden, A.F.A.; Majid, Z.A.; Matsumura, K.; Iqbal, A. A short review on electrochemical exfoliation of graphene and graphene quantum dots. *Carbon Lett.* **2021**, *31*, 371–388, https://doi.org/10.1007/s42823-020-00212-3.
[32] Li, Y.; Zhang, H.; Crespo, M.; Porwal, H.; Picot, O.; Santagiuliana, G.; Huang, Z.; Barbieri, E.; Pugno, N.M.; Peijs, T.; et al. In Situ Exfoliation of Graphene in Epoxy Resins: A Facile Strategy to Efficient and Large Scale Graphene Nanocomposites. *ACS Appl. Mater. Interfaces* **2016**, *8*, 24112–24122, https://doi.org/10.1021/acsami.6b07492.
[33] Wu, W.; Zhang, C.; Hou, S. Electrochemical exfoliation of graphene and graphene-analogous 2D nanosheets. *J. Mater. Sci.* **2017**, *52*, 10649–10660, https://doi.org/10.1007/s10853-017-1289-x.
[34] Kim, J.; Kim, J.; Song, S.; Zhang, S.; Cha, J.; Kim, K.; Yoon, H.; Jung, Y.; Paik, K.-W.; Jeon, S. Strength dependence of epoxy composites on the average filler size of non-oxidized graphene flake. *Carbon* **2016**, *113*, 379–386, https://doi.org/10.1016/j.carbon.2016.11.023.
[35] Sai, B.K.; Tambe, P. Fracture mechanism and scratch behaviour of MWNTs reinforced 70/30 (wt/wt) PC/ABS blends and their nanocomposites. *Adv. Ind. Eng. Polym. Res.* **2022**, *5*, 183–197, https://doi.org/10.1016/j.aiepr.2022.02.002.
[36] Pozdnyakov, A.O.; Brzhezinskaya, M.M.; Vinogradov, A.S.; Friedrich, K. NEXAFS Spectra of Polymer-nanocarbon Composites. *Full- Nanotub. Carbon Nanostructures* **2008**, *16*, 471–474, https://doi.org/10.1080/15363830802282409.
[37] Rahmat, M.; Hubert, P. Carbon nanotube–polymer interactions in nanocomposites: A review. *Compos. Sci. Technol.* **2011**, *72*, 72–84, https://doi.org/10.1016/j.compscitech.2011.10.002.
[38] Yu, A.; Ramesh, P.; Sun, X.; Bekyarova, E.; Itkis, M.E.; Haddon, R.C. Enhanced Thermal Conductivity in a Hybrid Graphite Nanoplatelet – Carbon Nanotube Filler for Epoxy Composites. *Adv. Mater.* **2008**, *20*, 4740–4744, https://doi.org/10.1002/adma.200800401.
[39] Yue, L.; Pircheraghi, G.; Monemian, S.A.; Manas-Zloczower, I. Epoxy composites with carbon nanotubes and graphene nanoplatelets – Dispersion and synergy effects. *Carbon* **2014**, *78*, 268–278, https://doi.org/10.1016/j.carbon.2014.07.003.
[40] Bisht, A.; Dasgupta, K.; Lahiri, D. Evaluating the effect of addition of nanodiamond on the synergistic effect of graphene-carbon nanotube hybrid on the mechanical properties of epoxy based composites. *Polym. Test.* **2019**, *81*, 106274, https://doi.org/10.1016/j.polymertesting.2019.106274.
[41] Georgakilas, V.; Otyepka, M.; Bourlinos, A.B.; Chandra, V.; Kim, N.; Kemp, K.C.; Hobza, P.; Zboril, R.; Kim, K.S. Functionalization of Graphene: Covalent and Non-Covalent Approaches, Derivatives and Applications. *Chem. Rev.* **2012**, *112*, 6156–6214, doi:10.1021/cr3000412.
[42] Naeem, M.; Kuan, H.-C.; Michelmore, A.; Meng, Q.; Qiu, A.; Aakyiir, M.; Losic, D.; Zhu, S.; Ma, J. A new method for preparation of functionalized graphene and its epoxy nanocomposites. *Compos. Part B: Eng.* **2020**, *196*, 108096, https://doi.org/10.1016/j.compositesb.2020.108096.

[43] Li, Z.; Wang, R.; Young, R.J.; Deng, L.; Yang, F.; Hao, L.; Jiao, W.; Liu, W. Control of the functionality of graphene oxide for its application in epoxy nanocomposites. *Polymer* **2013**, *54*, 6437–6446, https://doi.org/10.1016/j.polymer.2013.09.054.
[44] Wei, Y.; Hu, X.; Jiang, Q.; Sun, Z.; Wang, P.; Qiu, Y.; Liu, W. Influence of graphene oxide with different oxidation levels on the properties of epoxy composites. *Compos. Sci. Technol.* **2018**, *161*, 74–84, https://doi.org/10.1016/j.compscitech.2018.04.007.
[45] Meng, F.; Meng, Q.; Guo, F.; Alam, J.; Ma, J. Bismuthene nanosheets prepared by an environmentally friendly method and their thermoelectric epoxy nanocomposites. *Adv. Ind. Eng. Polym. Res.* **2023**, https://doi.org/10.1016/j.aiepr.2023.06.003.
[46] Peng, Q.; Tan, X.; Xiong, X.; Wang, Y.; Novotná, J.; Shah, K.V.; Stempień, Z.; Periyasamy, A.P.; Kejzlar, P.; Venkataraman, M.; et al. Insights into the large-size graphene improvement effect of the mechanical properties on the epoxy/glass fabric composites. *Polym. Compos.* **2023**, *44*, 7430–7443, https://doi.org/10.1002/pc.27635.
[47] Hu, H.; Zhao, B.; Itkis, M.E.; Haddon, R.C. Nitric Acid Purification of Single-Walled Carbon Nanotubes. *J. Phys. Chem. B* **2003**, *107*, 13838–13842, https://doi.org/10.1021/jp035719i.
[48] Bai, M.; Chen, J.; Wu, W.; Zeng, X.; Wang, J.; Zou, H. Preparation of stable aqueous dispersion of edge-oxidized graphene and its transparent conductive films. *Colloids Surfaces A: Physicochem. Eng. Asp.* **2016**, *490*, 59–66, https://doi.org/10.1016/j.colsurfa.2015.11.033.
[49] Park, J.K.; Kim, D.S. Effects of an aminosilane and a tetra-functional epoxy on the physical properties of di-functional epoxy/graphene nanoplatelets nanocomposites. *Polym. Eng. Sci.* **2013**, *54*, 969–976, https://doi.org/10.1002/pen.23624.
[50] Guerrero-Contreras, J.; Caballero-Briones, F. Graphene oxide powders with different oxidation degree, prepared by synthesis variations of the Hummers method. *Mater. Chem. Phys.* **2015**, *153*, 209–220, https://doi.org/10.1016/j.matchemphys.2015.01.005.
[51] Tian, S.; Sun, J.; Yang, S.; He, P.; Wang, G.; Di, Z.; Ding, G.; Xie, X.; Jiang, M. Controllable Edge Oxidation and Bubbling Exfoliation Enable the Fabrication of High Quality Water Dispersible Graphene. *Sci. Rep.* **2016**, *6*, 34127, https://doi.org/10.1038/srep34127.
[52] Tobiszewski, M.; Tsakovski, S.; Simeonov, V.; Namieśnik, J.; Pena-Pereira, F. A solvent selection guide based on chemometrics and multicriteria decision analysis. *Green Chem.* **2015**, *17*, 4773–4785, https://doi.org/10.1039/c5gc01615k.
[53] J.D. Chea, A. Christon, V. Pierce, J.H. Reilly, M. Russ, M. Savelski, C.S. Slater, K.M. Yenkie. Framework for solvent recovery, reuse, and recycling in industries. Comput. Aided Chem. Eng. 2019; 47: 199-204. https://doi.org/10.1016/B978-0-12-818597-1.50032-1
[54] Paton, K.R.; Varrla, E.; Backes, C.; Smith, R.J.; Khan, U.; O'Neill, A.; Boland, C.S.; Lotya, M.; Istrate, O.M.; King, P.; et al. Scalable production of large quantities of defect-free few-layer graphene by shear exfoliation in liquids. *Nat. Mater.* **2014**, *13*, 624–630, https://doi.org/10.1038/nmat3944.
[55] Brzhezinskaya, M.; Kapitanova, O.; Kononenko, O.; Koveshnikov, S.; Korepanov, V.; Roshchupkin, D. Large-scalable graphene oxide films with resistive switching for non-volatile memory applications. *J. Alloy. Compd.* **2020**, *849*, 156699, https://doi.org/10.1016/j.jallcom.2020.156699.
[56] Liu, L.; Zhang, J.; Zhao, J.; Liu, F. Mechanical properties of graphene oxides. *Nanoscale* **2012**, *4*, 5910–5916, https://doi.org/10.1039/c2nr31164j.
[57] Zhang, Y.; Wang, Y.; Yu, J.; Chen, L.; Zhu, J.; Hu, Z. Tuning the interface of graphene platelets/epoxy composites by the covalent grafting of polybenzimidazole. *Polymer* **2014**, *55*, 4990–5000, https://doi.org/10.1016/j.polymer.2014.07.045.
[58] Wan, Y.-J.; Tang, L.-C.; Gong, L.-X.; Yan, D.; Li, Y.-B.; Wu, L.-B.; Jiang, J.-X.; Lai, G.-Q. Grafting of epoxy chains onto graphene oxide for epoxy composites with improved mechanical and thermal properties. *Carbon* **2014**, *69*, 467–480, https://doi.org/10.1016/j.carbon.2013.12.050.
[59] Naebe, M.; Wang, J.; Amini, A.; Khayyam, H.; Hameed, N.; Li, L.H.; Chen, Y.; Fox, B. Mechanical Property and Structure of Covalent Functionalised Graphene/Epoxy Nanocomposites. *Sci. Rep.* **2014**, *4*, 4375, https://doi.org/10.1038/srep04375.
[60] Domun, N.; Hadavinia, H.; Zhang, T.; Liaghat, G.; Vahid, S.; Spacie, C.; Paton, K.R.; Sainsbury, T. Improving the fracture toughness properties of epoxy using graphene nanoplatelets at low filler content. *Nanocomposites* **2017**, *3*, 85–96, https://doi.org/10.1080/20550324.2017.1365414.
[61] Chong, H.M.; Hinder, S.J.; Taylor, A.C. Graphene nanoplatelet-modified epoxy: effect of aspect ratio and surface functionality on mechanical properties and toughening mechanisms. *J. Mater. Sci.* **2016**, *51*, 8764–8790, https://doi.org/10.1007/s10853-016-0160-9.
[62] Yasmin, A.; Daniel, I.M. Mechanical and thermal properties of graphite platelet/epoxy composites. *Polymer* **2004**, *45*, 8211–8219, https://doi.org/10.1016/j.polymer.2004.09.054.
[63] Zaman, I.; Kuan, H.-C.; Dai, J.; Kawashima, N.; Michelmore, A.; Sovi, A.; Dong, S.; Luong, L.; Ma, J. From carbon nanotubes and silicate layers to graphene platelets for polymer nanocomposites. *Nanoscale* **2012**, *4*, 4578–4586, https://doi.org/10.1039/c2nr30837a.

[64] Rafiee, M.A.; Rafiee, J.; Wang, Z.; Song, H.; Yu, Z.-Z.; Koratkar, N. Enhanced Mechanical Properties of Nanocomposites at Low Graphene Content. *ACS Nano* **2009**, *3*, 3884–3890, https://doi.org/10.1021/nn9010472.
[65] Bortz, D.R.; Heras, E.G.; Martin-Gullon, I. Impressive Fatigue Life and Fracture Toughness Improvements in Graphene Oxide/Epoxy Composites. *Macromolecules* **2011**, *45*, 238–245, https://doi.org/10.1021/ma201563k.
[66] Dutta, A.; Penumadu, D.; Files, B. Nanoindentation testing for evaluating modulus and hardness of single-walled carbon nanotube–reinforced epoxy composites. *J. Mater. Res.* **2004**, *19*, 158–164, https://doi.org/10.1557/jmr.2004.19.1.158.
[67] A. Moosa, A. Ramazani, M. Nabil. Mechanical and Electrical Properties of Graphene Nanoplates and Carbon-Nanotubes Hybrid Epoxy Nanocomposites. Am. J. Mater. Sci. 2016; 6(6): 157-165. https://doi.org/10.5923/j.materials.20160606.03
[68] Li, W.; Dichiara, A.; Bai, J. Carbon nanotube–graphene nanoplatelet hybrids as high-performance multifunctional reinforcements in epoxy composites. *Compos. Sci. Technol.* **2013**, *74*, 221–227, https://doi.org/10.1016/j.compscitech.2012.11.015.